Carbon Trends 15 (2024) 100334

Contents lists available at ScienceDirect

Carbon Trends

journal homepage: www.elsevier.com/locate/cartre

Adsorption of corannulene on graphene

Panyada Sripaturad [a], Ngamta Thamwattana [b,*], Amir Karton [c,*], Kyle Stevens [b], Duangkamon Baowan [a]

[a] Department of Mathematics, Faculty of Science, Mahidol University, Rama VI Rd., Bangkok 10400, Thailand
[b] School of Information and Physical Sciences, University of Newcastle, Callaghan, NSW 2308, Australia
[c] School of Science and Technology, University of New England, Armidale, NSW 2351, Australia

ARTICLE INFO

Keywords:
Graphene
Corannulene
Lennard-Jones potential
Continuum approach
Density functional theory
Pair-wise dispersion
Adsorption

ABSTRACT

Graphene has been used as a catalyst to reduce the energy barrier for corannulene inversion. For such a catalytic study, corannulene structures are normally assumed to already be in close proximity to graphene, either in the concave-up or concave-down orientation. Here we use both the Lennard-Jones potential (pair-wise dispersion model) and density functional theory calculations to show that corannulene at a distance further away from graphene can adopt various orientations to optimise its interaction with graphene.

1. Introduction

Corannulene ($C_{20}H_{10}$), also known as a buckybowl, consists of 20 carbon atoms formed into a bowl-shaped structure with 10 hydrogen atoms on the rim. The electronic and mechanical properties of a corannulene are distinct between its concave and convex surfaces making this molecule one of the highly studied hydrocarbon compounds. In particular, the bowl-to-bowl inversion phenomenon has attracted much research attention [1–3]. Many methods have been proposed to induce the bowl inversion, one of which is to reduce the inversion energy barrier by using 2D substrates (e.g. graphene) as a catalyst [4–6].

Graphitic surfaces have been used to adsorb planar and curved polycyclic aromatic hydrocarbons (PAHs) [4–21]. While Wang et al. [7] perform experiments to confirm the binding of naphthalene, phenanthrene, and pyrene on graphene and graphene oxide, other works in this area concentrate on using computational approach to model the mechanics of adsorption of different PAHs on graphene [4–6,8–21]. Commonly used computational methods include semi-empirical potential, ab initio calculations, empirical damping functions and density functional theory [5,8–11,13–16,18–20]. For curved PAHs, such as corannulene studied here, their interactions with graphene have been investigated mainly by density functional theory (DFT) calculations [4–6,19,20]. In particular, Karton [4,6] and Dennis [5] use DFT and double-hybrid DFT calculations to show that a single-layer graphene catalyst can reduce the energy barrier for the bowl-to-bowl inversion by at least 50%. Furthermore, Karton [6] gives the analysis of components of the intermolecular interaction energy and shows that dispersion energy dominates the corannulene-graphene interaction followed by the electrostatic interactions. These attractive interactions outweigh the Pauli repulsion [6].

The bowl-to-bowl inversion in corannulene occurs when corannulene is located at close proximity to the graphene surface, either in the concave-up or concave-down orientation [6,21]. However, at various distances away from graphene, corannulene may adopt other orientations to maximise its interaction with graphene. To confirm this hypothesis, this paper investigates the mechanics of adsorption of a corannulene molecule onto a graphene sheet. We follow the approach proposed in [12] which considers the adsorption of a polycyclic aromatic hydrocarbon (PAH) known as coronene ($C_{24}H_{12}$) on a graphitic surface. We note that coronene is a planar molecule, whereas corannulene studied here has a non-planar structure. According to [12], coronene at various distances from graphene adopts different orientations. We envisage that corannulene, as it approaches graphene, will also adopt various orientations in order to maximise the pair-wise interaction with graphene leading to minimum total energy.

Since the interaction considered here is physisorption, for which the intermolecular interactions are primarily governed by van der Waals forces [13,14], we use the Lennard-Jones potential and extend a hybrid-continuum approach proposed in [12,21] to obtain the pair-wise disper-

* Corresponding authors.
E-mail addresses: natalie.thamwattana@newcastle.edu.au (N. Thamwattana), amir.karton@une.edu.au (A. Karton).

https://doi.org/10.1016/j.cartre.2024.100334
Received 25 December 2023; Received in revised form 8 February 2024; Accepted 22 February 2024
Available online 1 March 2024

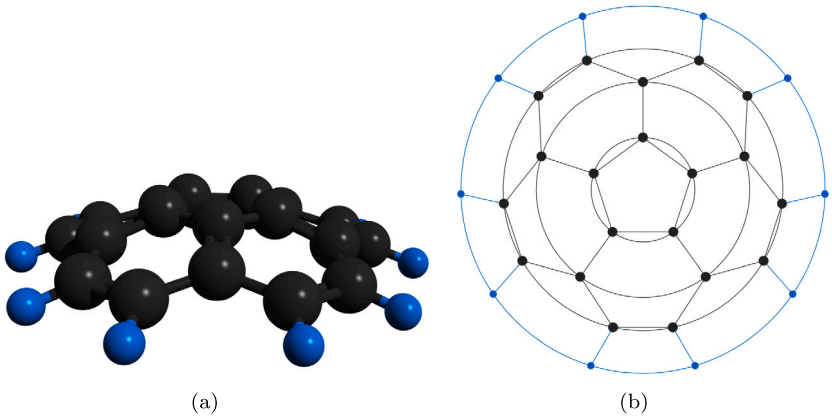

Fig. 1. Atomic structure of a corannulene (• carbon atoms, • hydrogen atoms): (a) side view showing bowl-shaped structure and (b) top view with fitted three inner circular rings of carbon atoms and an outer circular ring of hydrogen atoms.

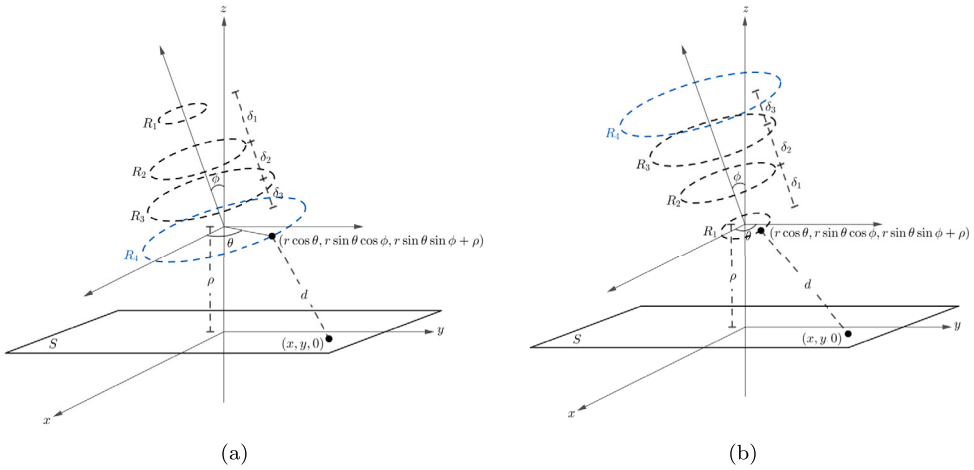

Fig. 2. The model for the interaction between tilted corannulene and graphene: (a) concave-down bowl and (b) concave-up bowl. Note that the distances between each ring in corannulene are given by $\delta_1 = 0.5442$ Å, $\delta_2 = 0.3624$ Å and $\delta_3 = 0.3822$ Å.

sion interaction energy between corannulene and graphene. We note that the model in [21] considers corannulene at close distances to graphene so the orientation of corannulene is assumed to be in the form of only concave-up or concave-down. Here, we introduce a new model where the interaction energy is a function of both the rotational angle of a corannulene and its distance from the graphene sheet. Minimising the energy for a given distance, we find favourable orientations at which the corannulene structure optimises its interaction with graphene. Therefore, this model can be used to inform the behaviour of corannulene as it approaches graphene, which may be useful not only for catalytic applications, but also for gas and pollutant adsorption technology.

In a continuum approach, we replace the summation of pairwise atomic interactions seen in a discrete approach by surface integrals of a potential function. To evaluate such integrals, assumption of the geometries of the interacting structures is required so that the surface elements, limits of integration and typical distances between two interacting surface elements can be determined. As such, a continuum approach is appropriate for regular shaped structures with well-defined geometries, such as nanotubes, fullerenes, nanocones and flat graphene sheets [22]. Hybrid discrete-continuum approach can also be applied, where one structure is treated as continuous, while the other is assumed to be a collection of discrete atoms or sub-structures. We note that the Lennard-Jones potential is commonly used in a continuum approach due to its simple functional form, which enables the integrals to be evaluated analytically. While this approach with the Lennard-Jones potential works reasonably well for isotropic structures and is able to provide qualitative agreement with dispersion-corrected density functional theory (DFT) calculations for interactions involving corannulenes [21,23], quantitatively the Lennard-Jones potential tends to give overbinding energy for anisotropic materials [24] and this is also shown here when we compare our results with dispersion-corrected DFT interaction energies. However, the advantage of continuum approach with the Lennard-Jones potential is the derivation of analytical expressions for the adsorption energy, which can be readily computed, analysed and visualised using an algebraic computer package, such as MAPLE.

This paper is structured as follows. In the following section, we mathematically model the adsorption of corannulene on graphene. Analytical expressions for the interaction energy are determined, where the detailed derivation is provided in Appendix A. In Section 3, numerical results from the pair-wise dispersion model are presented together with DFT calculations. Finally, conclusions and remarks are given in Section 4.

2. Interaction energy between corannulene and graphene

In order to use a continuum approach to determine the interaction energy between corannulene and graphene, we first need to approximate the geometries of both structures. Here, we assume that corannulene comprises four rings, where rings R_1 and R_2 each consists of five carbon atoms, ring R_3 consists of ten carbon atoms and the largest ring R_4 consists of ten hydrogen atoms (see Fig. 1). Each ring is centred on the same axis and tilted by a rotation angle ϕ from the z-axis, where $\phi \in [0, \pi/2]$ (see Fig. 2). The radius, circumference and atomic density of each ring are given in Table 1. For the graphene sheet, due to its

Table 1
Physical parameters of corannulene where r_i, c_i and η_i are the radius, circumference and mean atomic density of ring R_i, respectively.

	r_i (Å)	c_i (Å)	η_i (Å^{-1})
Carbon ring 1 (R_1)	1.2108	7.6074	0.6573
Carbon ring 2 (R_2)	2.4958	15.6818	0.3188
Carbon ring 3 (R_3)	3.2688	20.5384	0.4870
Hydrogen ring (R_4)	4.2572	26.7488	0.3738

large size compared to the diameter of corannulene, we model it as an infinite plane with uniform atomic surface density of carbon atoms.

Here, we consider the configurations of corannulene as shown in Fig. 2. In particular, Fig. 2(a) demonstrates the model for a concave-down bowl. We assume the centre of the hydrogen ring R_4 to be at $(0,0,\rho)$ and that the other rings are tilted such that the centres of rings R_3, R_2 and R_1 are given by $\left(0,-\delta_3\sin\phi,\rho+\delta_3\cos\phi\right)$, $\left(0,-(\delta_2+\delta_3)\sin\phi,\rho+(\delta_2+\delta_3)\cos\phi\right)$ and $\left(0,-(\delta_1+\delta_2+\delta_3)\sin\phi,\rho+(\delta_1+\delta_2+\delta_3)\cos\phi\right)$, respectively. Similarly, Fig. 2(b) shows the model for a concave-up bowl. Here, the centre of the smallest carbon ring R_1 is assumed to be located at $(0,0,\rho)$ so the centres of rings R_2, R_3 and R_4 become $\left(0,-\delta_1\sin\phi,\rho+\delta_1\cos\phi\right)$, $\left(0,-(\delta_1+\delta_2)\sin\phi,\rho+(\delta_1+\delta_2)\cos\phi\right)$ and $\left(0,-(\delta_1+\delta_2+\delta_3)\sin\phi,\rho+(\delta_1+\delta_2+\delta_3)\cos\phi\right)$, respectively. The values of δ_1, δ_2 and δ_3, which are given in Fig. 2, are based on the density functional theory calculation for the optimised geometries (Cartesian coordinates) of all atoms in corannulene [6].

By configuring the model as shown in Fig. 2, the total energy between the corannulene and the graphene sheet can consequently be calculated as the sum of four interactions including the three interactions of carbon rings with the graphene sheet and one interaction of the hydrogen ring with the graphene sheet. However, all four interactions are only specific cases of one general problem, namely the interaction between a circular ring and a plane. Here, we calculate the ring-plane interaction energy using the setup between graphene and its closest ring of corannulene, which can be seen in either Fig. 2(a) or (b). For such a problem, we assume that the graphene sheet is a flat surface on the $xy-$plane, so the coordinates of its typical point are given by $(x,y,0)$. For a ring of radius r centred at $(0,0,\rho)$ with a titled angle ϕ, the coordinates of a typical point on the ring are given by $(r\cos\theta, r\sin\theta\cos\phi, r\sin\theta\sin\phi+\rho)$ where $\theta\in[0,2\pi]$. Thus, the distance between the two typical points is given by

$$d^2=(r\cos\theta-x)^2+(r\sin\theta\cos\phi-y)^2+(r\sin\theta\sin\phi+\rho)^2. \tag{1}$$

Using the Lennard-Jones potential and a continuum approach, the interaction energy can be determined from

$$E(\rho,\phi)=\eta_g\eta_r r\int_0^{2\pi}\int_{-\infty}^{\infty}\int_{-\infty}^{\infty}\left(-\frac{A}{d^6}+\frac{B}{d^{12}}\right)dx\,dy\,d\theta=\eta_g\eta_r r\left(-AI_3+BI_6\right), \tag{2}$$

where A and B are the attractive and repulsive constants, respectively, and η_g and η_r denote the surface density of graphene and the line density of the ring, respectively. The distance d is defined in (1) and

$$I_n=\int_0^{2\pi}\int_{-\infty}^{\infty}\int_{-\infty}^{\infty}d^{-2n}dx\,dy\,d\theta,$$

where $n=3,6$. The integral I_n was evaluated in Tran-Duc et al. [12], however, we restate the detailed calculation in Appendix A of this paper for the sake of completeness.

Based on (2) and by taking into account all four rings of corannulene, the total interaction energy is given by

Table 2
The values of the attractive and repulsive constants for carbon-carbon and carbon-hydrogen interactions used in this paper.

Interaction	A_i (kJ mol^{-1} Å^6)	B_i (kJ mol^{-1} Å^{12})
C-C	2865.84	4673725.47
C-H	830.93	606947.72

$$E_{total}(\rho,\phi)=\eta_g\sum_{i=1}^{4}\eta_i r_i(-A_iI_3+B_iI_6), \tag{3}$$

where $\eta_g=0.3812$ Å^{-2} is the atomic density of graphene sheet and η_i is the line atomic density of the ring R_i for which the values are given in Table 1. For the attractive and repulsive constants, $A_i=A_{C-C}$ and $B_i=B_{C-C}$ when $i=1,2,3$ and $A_i=A_{C-H}$ and $B_i=B_{C-H}$ when $i=4$. The values of these constants are prescribed in Table 2, which are based on the values of the well depth and van der Waals distance given in Rappe et al. [25]. As shown in Appendix A, the integral I_n has the form,

$$I_n(\rho)=\frac{2\pi^2}{n-1}\left(r_i\sin\phi+(\rho+\epsilon_i)\right)^{-2n+2}F\left(2n-2,\frac{1}{2};1;\frac{2r_i\sin\phi}{r_i\sin\phi+(\rho+\epsilon_i)}\right), \tag{4}$$

where $n=3,6$, r_i is the radius of Ring R_i and $F(a,b;c;z)=\sum_{k=0}^{\infty}\frac{(a)_k(b)_k}{k!(c)_k}z^k$ is the hypergeometric function where $(a)_k=a(a+1)(a+2)...(a+k-1)$ is the Pochhammer symbol. We note that ϵ_i $(i=1,2,3,4)$ denote the vertical distances from ρ to Ring R_i. For the concave-down bowl shown in Fig. 2(a), $\epsilon_1=0$, $\epsilon_2=\delta_3\cos\phi$, $\epsilon_3=(\delta_3+\delta_2)\cos\phi$ and $\epsilon_4=(\delta_3+\delta_2+\delta_1)\cos\phi$. Similarly, for the case of concave-up bowl presented in Fig. 2(b), $\epsilon_1=0$, $\epsilon_2=\delta_1\cos\phi$, $\epsilon_3=(\delta_1+\delta_2)\cos\phi$ and $\epsilon_4=(\delta_1+\delta_2+\delta_3)\cos\phi$. Further, we comment that this model can also be used for the interaction of graphene and a planar corannulene (its transition state structure), by letting $\epsilon_i=0$ for all i since all rings are concentric sharing the same centre at $(0,0,\rho)$. However, this case is not presented here since the transition state of corannulene only exists when the molecule is at a close distance to graphene, as mentioned in [21].

In the next section, we use (3) and (4) to determine the favourable configurations of corannulene at various distances ρ from the graphene sheet.

3. Numerical results and DFT calculations

In this section, we determine favourable orientations of corannulene corresponding to its distance ρ from graphene sheet. We note that ρ denotes the vertical distance measuring from graphene on the $xy-$plane to the centre of the closest ring of corannulene, which is R_4 for concave-down bowl and R_1 for concave-up bowl, as shown in Fig. 2. In the following subsections, we present results based on the two configurations shown in Fig. 2. The first scenario is when the corannulene is tilted from the concave-down bowl by an angle ϕ, where $\phi\in[0,\pi/2]$ (Fig. 2(a)). Correspondingly, when $\phi=0$ we have a fully concave-down bowl, and when $\phi=\pi/2$, we have a standing corannulene. The second scenario is when the corannulene is tilted from the concave-up bowl by an angle ϕ, where $\phi\in[0,\pi/2]$ (Fig. 2(b)). Correspondingly, when $\phi=0$ we have a fully concave-up bowl, and when $\phi=\pi/2$, we have a standing corannulene. We note that when $\phi=\pi/2$, both scenarios give to the same standing configuration.

3.1. Concave-down bowl

For the first scenario, we first plot the interaction energy (3) between corannulene and graphene as a function of the intermolecular

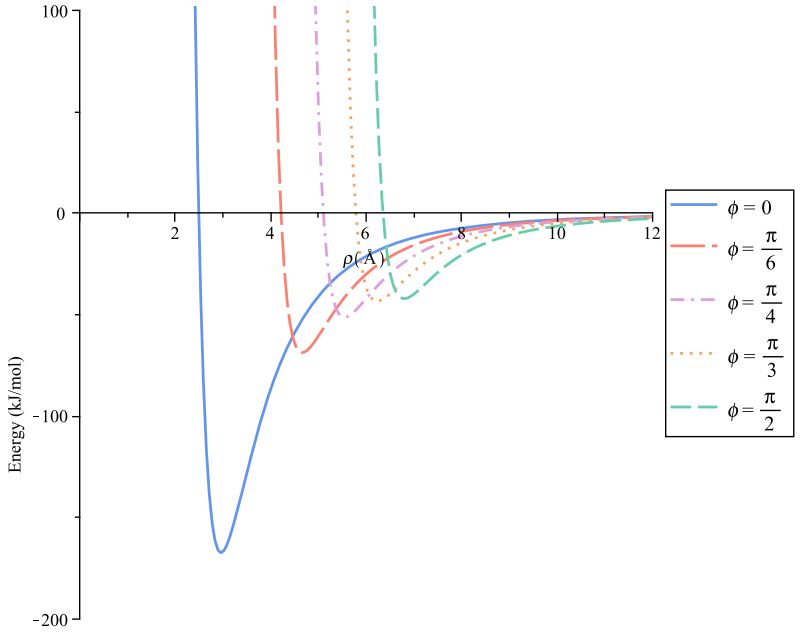

Fig. 3. The profiles of the interaction energy between concave-down corannulene and graphene sheet with various values of ϕ.

distance ρ for prescribed values of ϕ (Fig. 3). Due to the global minimum energy, concave-down corannulene ($\phi = 0$) near grahpene is the most stable configuration. However, for other values of ϕ, there exist local minimum energies. This implies that corannulene can adopt different orientations when the molecule is further away from the graphene sheet.

Next, we separately investigate three intervals of ρ, which lead to corannulene adopting fully concave-down, tilted concave-down and standing configurations, respectively. In Fig. 4, we show that at close distances to graphene, 2.4933 Å $< \rho <$ 3.4336 Å, coronnulene prefers to adopt the concave-down bowl ($\phi = 0$). We note that when $\phi = 0$, the lowest minimum energy of -167.3 kJ/mol occurs at $\rho = 2.9591$ Å. In Fig. 5 and Table 3, we see that the corannulene is tilted from the concave-down bowl with $0 < \phi < \pi/2$ when $\rho \in (3.4336, 6.6458)$. We note that in Fig. 5(a) and (b), we only plot 6.2 Å $< \rho <$ 6.5 Å so it is clear to see the dip in the energy profile. For $\rho > 6.6458$ Å, Fig. 6 shows that corannulene prefers its standing orientation ($\phi = \pi/2$). We note that the lowest minimum energy in this interval is -42.1 kJ/mol which corresponds to $\rho = 6.7974$ Å.

In Table 3, when ρ increases, we see an increasing in ϕ from 0 to $\pi/2$, and the minimum energy also increases from -167.3 kJ/mol to -39.9 kJ/mol. This table indicates that a corannulene prefers its arrangement as a concave-down bowl when it is near a graphene sheet. As the intermolecular distance increases, the concave-down bowl begins to tilt until it reaches a standing configuration when it is approximately 7 Å from the graphene sheet. Accordingly, we provide a diagram as shown in Fig. 7 to summarise possible orientations of a concave-down corannulene, which can occur by varying its distance from the graphene sheet. The minimum energy corresponding to the distance ρ where corannulene begins to change its orientation is also presented in this figure.

Table 3
Numerical values of the minimum interaction energy for a concave-down corannulene corresponding to particular angle ϕ and distance ρ from graphene sheet predicted by the pair-wise dispersion and PW6B95-D4 simulations (interaction energies are given in kJ/mol). (* denotes the global minimum energy.)

ρ (Å)	ϕ (rad)	Pair-wise Disp.	PW6B95-D4
2.9591	0	-167.3*	
3	0	-166.8	-82.0
3.5	0.0866	-128.2	
4	0.2844	-95.3	
5	0.5797	-62.0	-25.7
6	0.9168	-46.0	
6.5	1.1637	-41.5	
7	$\pi/2$	-39.9	-19.9

3.2. Concave-up bowl

Here, we investigate the second scenario where the concave-up bowl is rotated by ϕ, where $\phi \in [0, \pi/2]$. First, we plot Fig. 8 for the interaction energy between the corannulene and graphene shown in Fig. 2(b) as a function of the intermolecular distance ρ for given values of ϕ. Due to the global minimum energy, the fully concave-up bowl ($\phi = 0$) near the graphene sheet is the most stable configuration. However, for other angles ϕ, there exists the values of ρ that give rise to local minimum energies. This implies that corannulene can adopt different orientations rather than the concave-up bowl when the structure is further away from the graphene sheet.

Next, we determine three intervals of the distance ρ, which lead to corannulene favouring fully concave-up, tilted concave-up and standing configurations, respectively. For 2.6833 Å $< \rho <$ 3.2536 Å, the concave-up bowl ($\phi = 0$) is the preferable configuration. Fig. 9 shows that for ρ in this interval, $\phi = 0$ gives rise to the minimum energy. We obtain that the lowest minimum energy of -129.7 kJ/mol occurs at $\rho = 3.16342$ Å. Next, for 3.2536 Å $< \rho <$ 6.8727 Å, corannulene favours the tilted concave-up bowl configuration, where $0 < \phi < \pi/2$ as shown in Fig. 10. We note that in Fig. 10(a) and (b), we only plot 5.5 Å $< \rho <$ 6.8 Å so it is clear to see the dip in the energy profile. Finally, for $\rho > 6.8727$ Å, the standing configuration ($\phi = \pi/2$) is favourable as shown in Fig. 11. The lowest minimum energy in this interval is -42.1 kJ/mol corresponding to $\rho = 6.7974$ Å.

In Table 4, the minimum interaction energy corresponding to different values of ρ and ϕ are given. This demonstrates that an increasing in ρ leads to an increasing in ϕ from 0 to $\pi/2$, and the minimum energy also increases. This table indicates that a corannulene is likely to adopt a concave-up bowl when it is near a graphene sheet. As the intermolecular distance increases, the concave-up bowl starts to tilt until

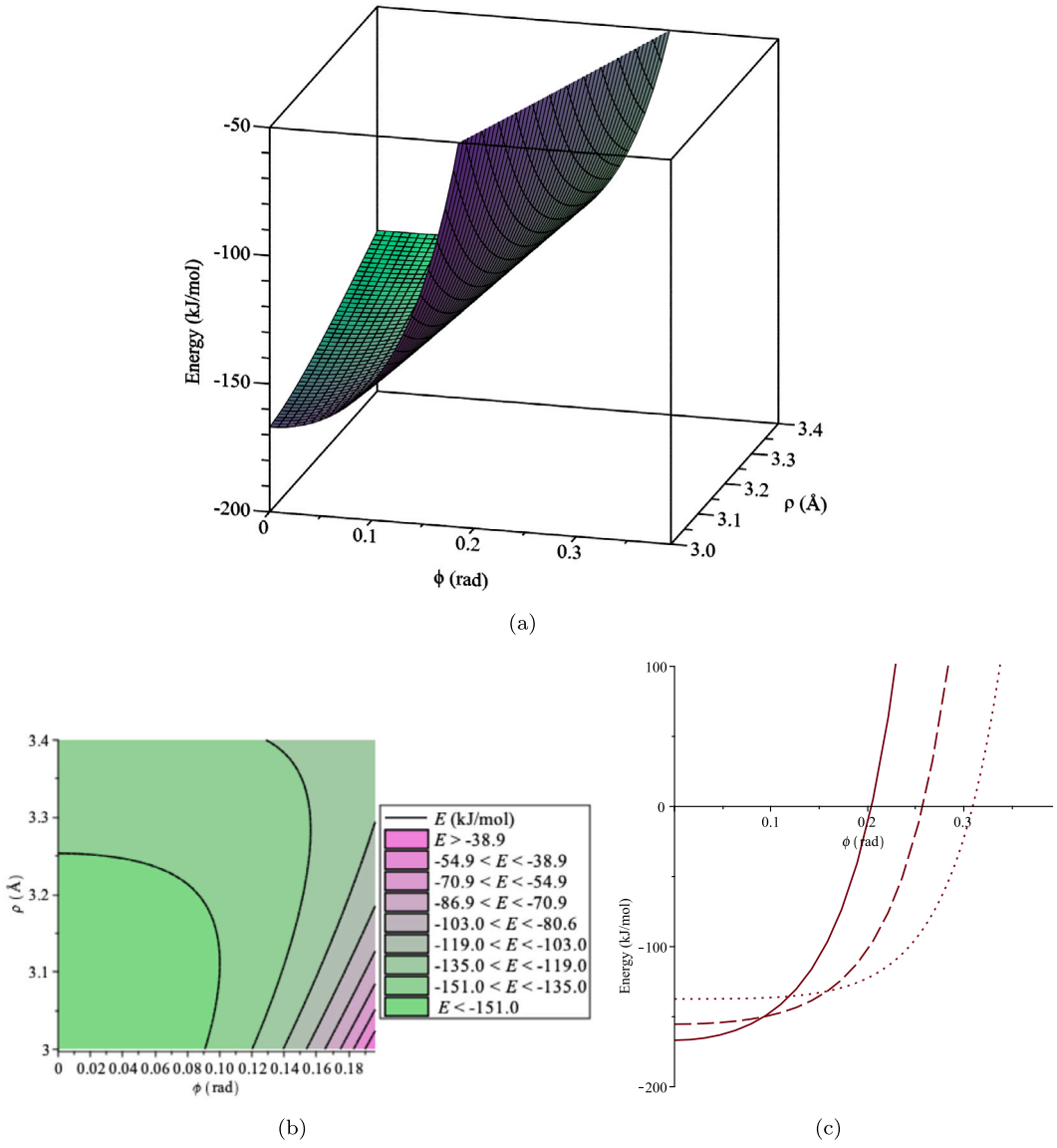

Fig. 4. The interaction energy between corannulene and graphene showing that for 3 Å $< \rho <$ 3.4 Å, the energy is minimised when $\phi = 0$ confirming that the concave-down bowl is the favourable configuration for this interval of ρ: (a) The total interaction energy as a function of ρ and ϕ, (b) Contour plot of the energy shown in (a) (the brightest green is the lowest energy region corresponding to ϕ close to 0), and (c) The total energy as a function of ϕ for fixed values of $\rho = 3$ Å (solid line), $\rho = 3.2$ Å (dash line) and $\rho = 3.4$ Å (dotted line).

it reaches a standing configuration. Based on this table, we present a diagram as shown in Fig. 12 to summarise possible orientations of a concave-up corannulene, which can occur by varying its distance from the graphene sheet. The minimum energy corresponding to the distance ρ where corannulene begins to change its orientation is also presented in this figure.

It is of interest to explore the above interaction energies obtained from our pair-wise dispersion model using rigorous quantum mechanical simulations. For this purpose, we performed DFT calculations at the PW6B95-D4/def2-TZVPP level of theory [26,27]. The PW6B95 exchange-correlation functional has been benchmarked and found to be robust for reaction and interaction energies involving related systems [18,19,28–33]. The atomic-charge dependent D4 dispersion correction was used to account for long-range van der Waals interaction [34,35]. The reported interaction energies were corrected for basis set superposition error (BSSE) in conjunction with the def2-TZVPP basis set [36–38]. All calculations were carried out using the Gaussian 16 program suite [39]. Following the same approach as in our previous DFT simulations [6,18,40], the graphene surface is modelled using a large $C_{96}H_{24}$ graphene nanoflake. We note that together with corannulene ($C_{20}H_{10}$), each graphene–corannulene model system includes 116 carbon atoms and 34 hydrogens (i.e., 730 electrons). Due to the high computational cost of these DFT simulations, we have only sampled three concave-down and three concave-up complexes at various intermolecular separations. The PW6B95-D4 results are presented in Tables 3 and 4. In these simulations, we use the $C_{96}H_{24}$ and $C_{20}H_{10}$ fragments that are optimised separately, however, the geometry of the $C_{96}H_{24}$•••$C_{20}H_{10}$ dimers is not optimised and the intermolecular distances and orientations are taken from the above pair-wise dispersion simulations. We note that the fully optimised $C_{96}H_{24}$•••$C_{20}H_{10}$ dimers have been considered by the authors previously [21] and, as expected, lead to larger interaction energies. It is important to note that in the fully optimised $C_{96}H_{24}$•••$C_{20}H_{10}$ dimers, the $C_{96}H_{24}$ graphene nanoflake is no longer planar. Namely, it adopts a shallow bowl structure with a bowl depth of 0.7935 Å in the concave-up complex and 0.4056 Å in the concave-down complex (see also ref. [40] for a discussion of the dip created in large graphene nanoflakes by the interaction with a benzene molecule).

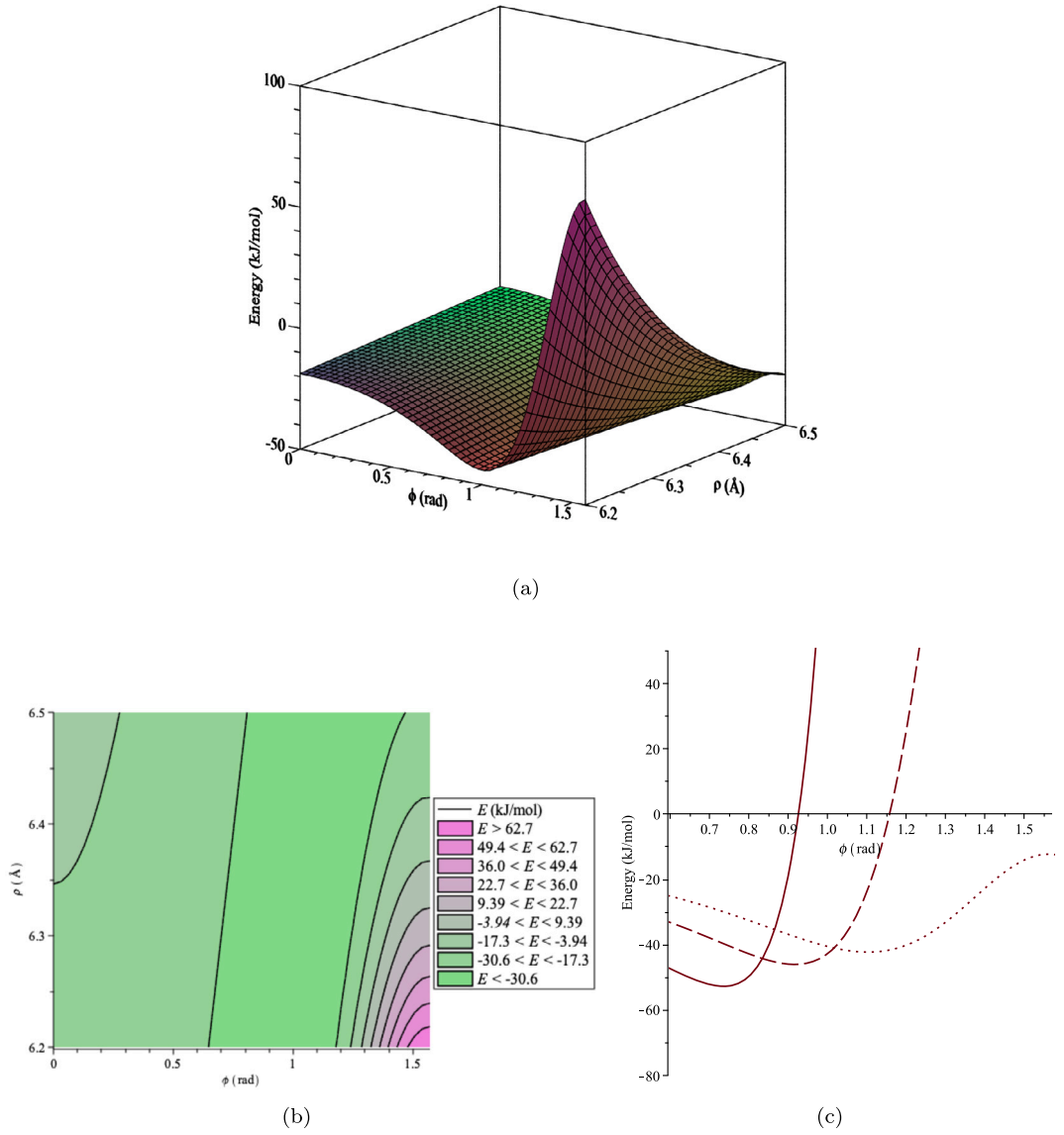

Fig. 5. The interaction energy between corannulene and graphene showing that for 6.2 Å $< \rho <$ 6.5 Å, the energy is minimised when $0 < \phi < \pi/2$ confirming that the tilted concave-down bowl is the favourable configuration for this interval of ρ: (a) The total interaction energy as a function of ρ and ϕ, (b) Contour plot of the energy shown in (a) (the brightest green is the lowest energy region corresponding to $0 < \phi < \pi/2$), and (c) The total energy as a function of ϕ for fixed values of $\rho = 5.5$ Å (solid line), $\rho = 6.0$ Å (dash line) and $\rho = 6.4$ Å (dotted line).

Table 4
Numerical values of the minimum interaction energy for a concave-up corannulene corresponding to particular angle ϕ and distance ρ from graphene sheet predicted by the pair-wise dispersion and PW6B95-D4 simulations (interaction energies are given in kJ/mol). (* denotes the global minimum energy.)

ρ (Å)	ϕ (rad)	Pair-wise Disp.	PW6B95-D4
3	0	-121.8	-51.2
3.1634	0	-129.7*	
3.5	0.2892	-119.8	
4	0.5025	-101.2	
5	0.8231	-71.6	-30.8
6	1.1471	-52.7	
6.5	1.3493	-45.8	
7	$\pi/2$	-39.9	-18.8

A comparison of the PW6B95-D4 and pair-wise dispersion model interaction energies reveals that there is a qualitative (but not quantitative) agreement between the two sets of results. In particular, the latter tend to overestimate the former by 50% or more (see Tables 3 and 4). Both models predict that the interaction energy is reduced significantly as the distance between the graphene and corannulene increases. However, more importantly, both models predict that for a fixed intermolecular separation, the concave-down complex is more stable than the concave-up complex. The energetic stability of the concave-down complex relative to the concave-up complex is reduced with the intermolecular separation. We note that there is a generally good quantitative agreement between the two theoretical models regarding the energetic stability of the concave-down complex relative to the concave-up complex. In particular, for $\rho = 3.0$ Å, we obtain that the concave-down complex is more stable than the concave-up complex by 45.0 (pair-wise dispersion) and 30.8 (PW6B95-D4) kJ/mol. For $\rho = 5.0$ Å, we obtain that the concave-down complex is more stable than the concave-up complex by 9.6 (pair-wise dispersion) and 5.1 (PW6B95-D4) kJ/mol. For $\rho = 7.0$ Å, the pair-wise dispersion interaction energies of the two

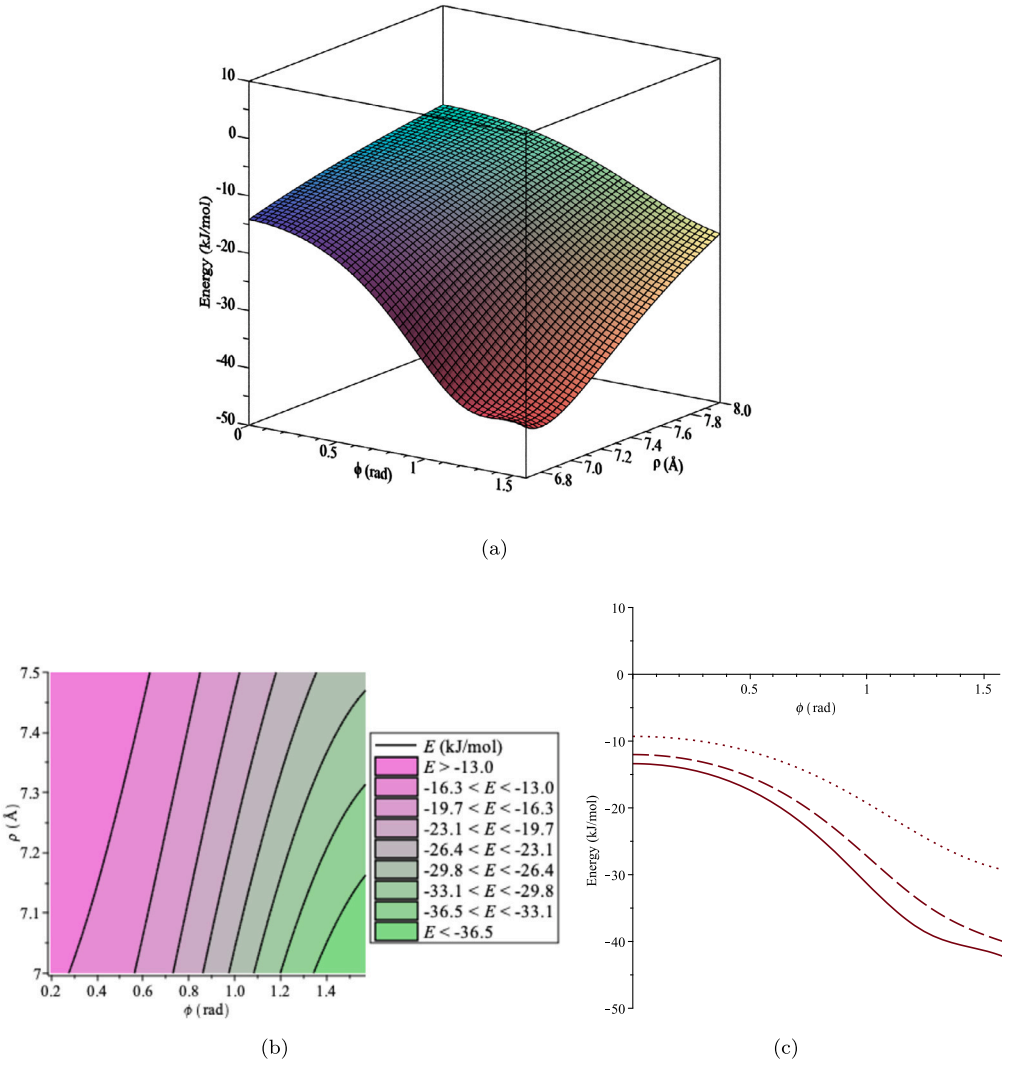

Fig. 6. The interaction energy between corannulene and graphene showing that for $\rho > 6.6$ Å, the energy is lowest when $\phi = \pi/2$ confirming that the standing orientation is the favourable configuration for this interval of ρ: (a) The total interaction energy as a function of ρ and ϕ, (b) Contour plot of the energy shown in (a) (the brightest green is the lowest energy region corresponding to ϕ close to $\pi/2$), and (c) The total energy as a function of ϕ for fixed values of $\rho = 6.8$ Å (solid line), $\rho = 7$ Å (dash line) and $\rho = 7.5$ Å (dotted line).

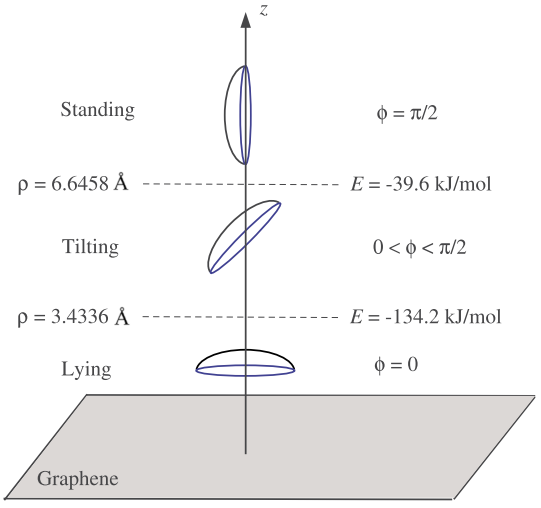

Fig. 7. Schematic diagram showing favourable orientations of corannulene concave-down bowl as the distance ρ from graphene sheet varies.

complexes are identical by definition, whereas the PW6B95-D4 simulations predict a very small energetic difference of 1.1 kJ/mol, due to the finite size of the graphene nanoflake. Inspection of Tables 3 and 4 also reveals that the absolute PW6B95-D4 interaction energies are significantly smaller than those predicted by the pair-wise dispersion model. In general, the PW6B95-D4 interaction energies are about half of the pair-wise dispersion interaction energies. These differences are attributed to the tendency of the pair-wise dispersion model to overestimate the interaction energies [21] and to the use of a graphene nanoflake in the PW6B95-D4 simulations. We expect that the use of a larger graphene nanoflake in the PW6B95-D4 simulations would result in larger interaction energies (see [40] for a detailed discussion of the effect of the size of the graphene nanoflake on the interaction energies). Calculating the interaction energies for $C_{150}H_{30}$•••$C_{20}H_{10}$ dimers at the above level of theory (PW6B95-D4/def2-TZVPP + BSSE corrections) is beyond the computational resources currently available to us. However, we can estimate the increase in the interaction energies when moving from a $C_{96}H_{24}$ to a $C_{150}H_{30}$ nano-graphene at the PW6B95-D4/def2-SVP level of theory. While this lower level of theory results in overbinding of the dimers, the difference between the $C_{96}H_{24}$•••$C_{20}H_{10}$ and $C_{150}H_{30}$•••$C_{20}H_{10}$ interaction energies should provide a useful estimation of effect of the size of the graphene flake on the interaction

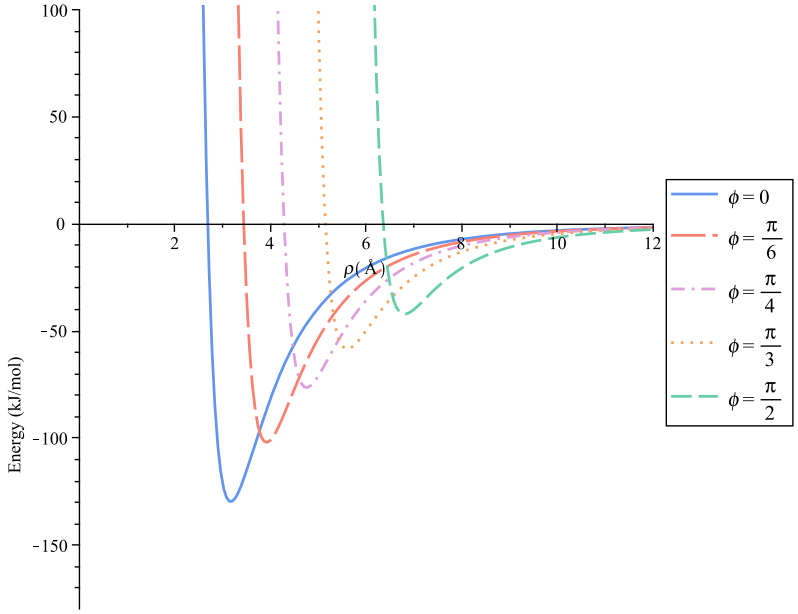

Fig. 8. The profiles of the interaction energy between concave-up corannulene and graphene sheet with various values of ϕ.

energies. When moving from a $C_{96}H_{24}$ to a $C_{150}H_{30}$ nano-graphene the interaction energies increase by merely 1.7 and 2.9 kJ/mol for the $\rho = 3.0$ Å dimers. As such, we can say that there is no significant effect when increasing the size of graphene. We also note that Dennis [16] showed that the adsorption energy of helicene (a non-planar PAH) on graphene only increases by $0.3 - 0.4$ kcal/mol when increasing the size of graphene from 6×6 unit cell to 7×7 unit cell. Therefore, the size of the graphene nanoflake used in the DFT simulations is unlikely to account for the discrepancy between the pair-wise dispersion model and PW6B95-D4 interaction energies. We note that the Lennard-Jones potential tends to overestimate the interaction energy and does not accurately model the Pauli repulsion, including for anisotropic structures with large π systems for which the Pauli repulsion may become significant [24,41,42]. Exploring different semi-empirical potentials for anisotropic structures that are suitable for a continuum modelling approach provides scope for future research.

4. Concluding remarks

This paper uses the Lennard-Jones potential and a continuum approach to determine the interaction energy between a corannulene and a graphene sheet. The interaction energy obtained depends on the distance ρ between graphene and corannulene and the rotation angle ϕ, which represents how much the molecule is tilted from the concave-up or concave-down position. For a given distance ρ, we can determine the orientation (i.e. the angle ϕ) such that the corrannulene optimises the interaction giving rise to minimum energy configuration. Similarly, for a given rotation angle ϕ, we can find the distance ρ that gives rise to the minimum energy for that particular orientation. In Fig. 13, we present a diagram showing the three intervals of ρ, which correspond to the three possible configurations of a corannulene, namely lying, tilting and standing, for both concave-down and concave-up bowls. We comment that in term of length scales, the three intervals shown in Fig. 13 are consistent between the two scenarios of concave-down and concave-up bowls. For each of these intervals, it is demonstrated here that corannulene can adopt either structures. However, at a close distance to graphene we predict that the fully concave-down bowl is the preferred configuration since it has the lowest minimum energy. Our findings here are in agreement with Maruyama and Okada [17] who use the STATE package based DFT and vdW-DF2 with the C09 exchange-correlation functional for dispersive interaction to show that at a fixed distance from graphene, corannulene favours two arrangements, namely the concave-down (hydrogenated rim facing graphene) and concave-up bowls. Among these, the interaction energy is lower for the concave-down structure. Also, we agree with [17] that the standing configuration has highest interaction energy.

We compare the interaction energies obtained from our pair-wise dispersion model with those obtained from PW6B95-D4 calculations and show that both models predict that for a fixed intermolecular separation the concave-down complex is energetically more stable than the concave-up complex, and that there is qualitative (but not quantitative) agreement between the two theoretical models. Consistent with our previous findings [21], the pair-wise dispersion model tends to overestimate the absolute interaction energies. Finally, we comment that the mechanics of adsorption of corannulene on graphene studied in this paper may be useful for future applications of corannulene, which require controlling the charge distribution by adjusting its configurations or locations of the graphene substrate.

CRediT authorship contribution statement

Panyada Sripaturad: Writing – original draft, Visualization, Software, Methodology, Investigation, Formal analysis. **Ngamta Thamwattana:** Writing – review & editing, Writing – original draft, Visualization, Supervision, Resources, Project administration, Methodology, Investigation, Formal analysis, Data curation, Conceptualization. **Amir Karton:** Writing – review & editing, Writing – original draft, Visualization, Validation, Software, Methodology, Investigation, Formal analysis, Conceptualization. **Kyle Stevens:** Visualization, Software, Methodology, Investigation, Conceptualization. **Duangkamon Baowan:** Writing – original draft, Visualization, Supervision, Resources, Investigation, Funding acquisition, Formal analysis.

Declaration of competing interest

The authors declare that they have no known competing financial interests or personal relationships that could have appeared to influence the work reported in this paper.

Data availability

Data will be made available on request.

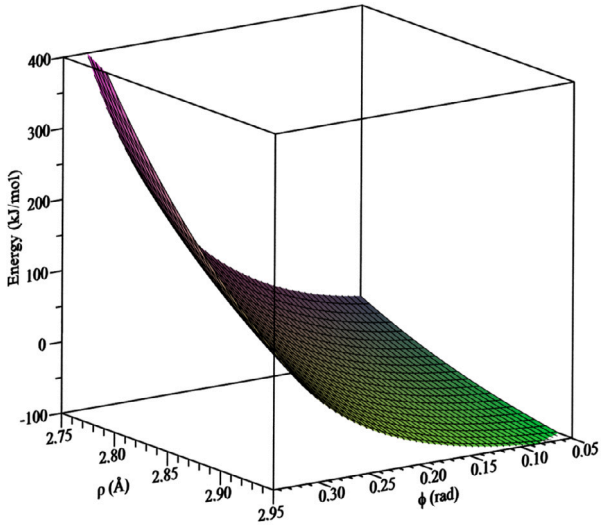

(a)

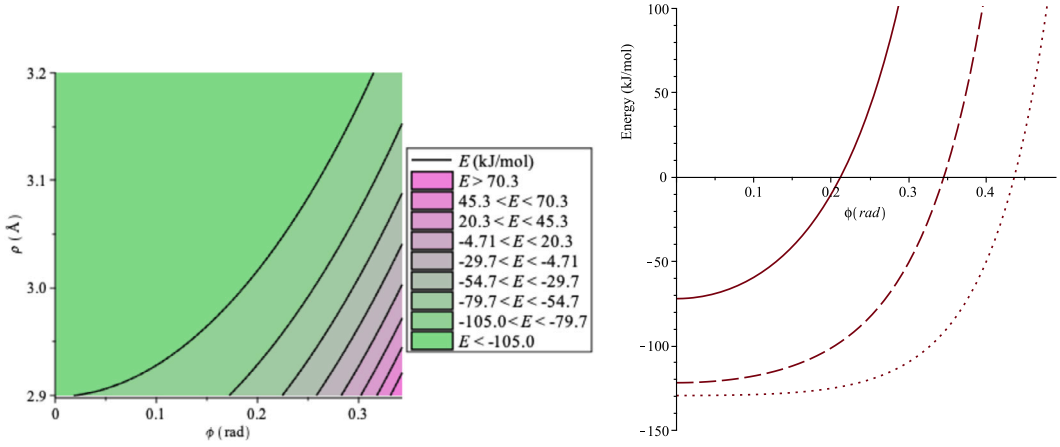

(b) (c)

Fig. 9. The interaction energy between corannulene and graphene showing that for 2.6 Å $< \rho <$ 3.2 Å, the energy is minimised when $\phi = 0$ confirming that the concave-up bowl is the favourable configuration for this interval of ρ: (a) The total interaction energy as a function of ρ and ϕ, (b) Contour plot of the energy shown in (a) (the brightest green is the lowest energy region corresponding to ϕ close to 0), and (c) The total energy as a function of ϕ for fixed values of $\rho = 2.8$ Å (solid line), $\rho = 3$ Å (dash line) and $\rho = 3.2$ Å (dotted line).

Acknowledgement

P.S. is grateful for the financial support of the Development and Promotion of Science and Technology Talents Project (DPST), Thailand. The authors also acknowledge the School of Information and Physical Sciences at the University of Newcastle for hosting the research visits by P.S. and D.B. The present work was undertaken with the assistance of resources from the National Computational Infrastructure (NCI), which is supported by the Australian Government.

Appendix A. Evaluation of I_n

The integral I_n is given by

$$I_n = \int_0^{2\pi}\int_{-\infty}^{\infty}\int_{-\infty}^{\infty} \frac{dx\,dy\,d\theta}{\left[(r\cos\theta - x)^2 + (r\sin\theta\cos\phi - y)^2 + (r\sin\theta\sin\phi + \rho)^2\right]^n},$$

where $n = 3, 6$. Letting $M = r\cos\theta - x$, $N = r\sin\theta\cos\phi - y$ and $z = r\sin\theta\sin\phi + \rho$, we have

$$I_n = \int_0^{2\pi}\int_{-\infty}^{\infty}\int_{-\infty}^{\infty} \frac{1}{(M^2 + N^2 + z^2)^n}\, dM\,dN\,d\theta.$$

Then, we make a substitution $M = \sqrt{N^2 + z^2}\tan\psi$ and get

$$I_n = \int_0^{2\pi}\int_{-\infty}^{\infty}\int_{-\pi/2}^{\pi/2} \frac{1}{[(N^2 + z^2)\sec^2\psi]^n}\sqrt{N^2 + z^2}\sec^2\psi\; d\psi\,dN\,d\theta,$$

which can be reduced to

$$I_n = \int_0^{2\pi}\int_{-\infty}^{\infty}(N^2 + z^2)^{1/2-n}\int_{-\pi/2}^{\pi/2}\cos^{2n-2}\psi\; d\psi\,dN\,d\theta. \tag{5}$$

Using the fact that

$$\int_0^{\pi/2}\cos^n\theta\; d\theta = \begin{cases} \frac{\pi}{2}\cdot\frac{(2m-1)!!}{(2m)!!} & \text{when } n = 2m, \\ \frac{(2m)!!}{(2m+1)!!} & \text{when } n = 2m+1, \end{cases}$$

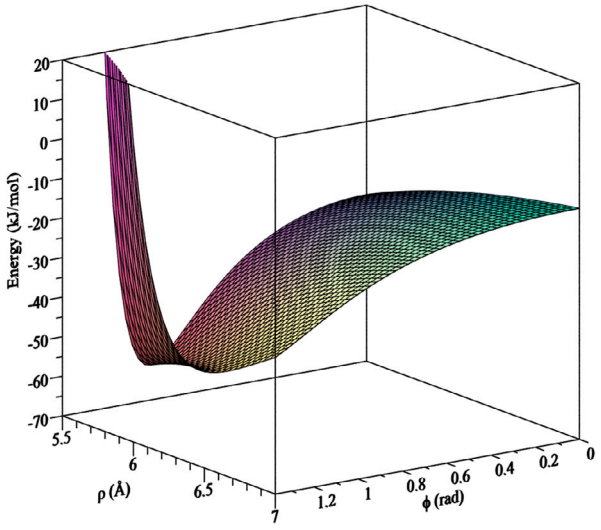

(a)

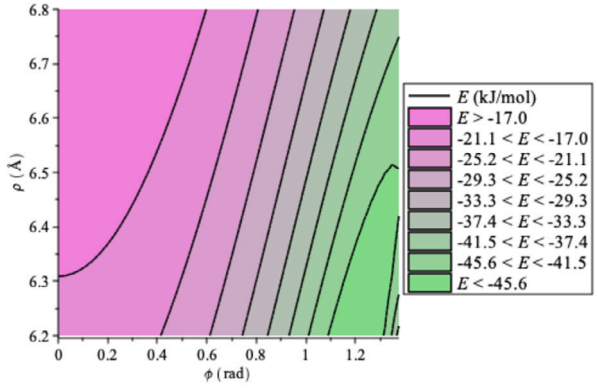

(b)

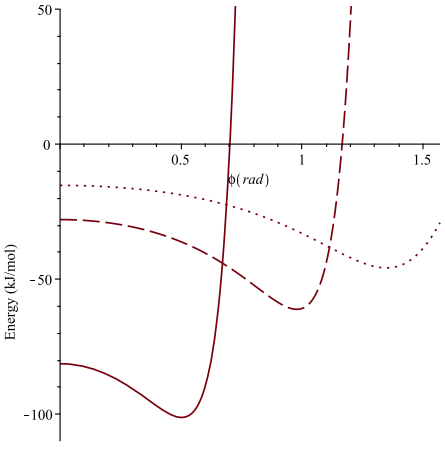

(c)

Fig. 10. The interaction energy between corannulene and graphene showing that for 5.5 Å $< \rho <$ 6.8 Å, the energy is minimised when $0 < \phi < \pi/2$ confirming that the tilted concave-up bowl is the favourable configuration for this interval of ρ: (a) The total interaction energy as a function of ρ and ϕ, (b) Contour plot of the energy shown in (a) (the brightest green is the lowest energy region corresponding to $0 < \phi < \pi/2$), and (c) The total energy as a function of ϕ for fixed values of $\rho = 4$ Å (solid line), $\rho = 5.5$ Å (dash line) and $\rho = 6.5$ Å (dotted line).

equation (5) becomes

$$I_n = \frac{(2n-3)!!\pi}{2^{n-1}(n-1)!}\int_0^{2\pi}\int_{-\infty}^{\infty}(N^2+z^2)^{1/2-n}\,dN\,d\theta.$$

Next, we substitute $N = z\tan\zeta$ and obtain

$$I_n = \frac{(2n-3)!!\pi}{2^{n-1}(n-1)!}\int_0^{2\pi}\int_{-\pi/2}^{\pi/2}(z^2\sec^2\zeta)^{1/2-n}(z\sec^2\zeta)\,d\zeta d\theta$$

$$= \frac{(2n-3)!!\pi}{2^{n-1}(n-1)!}\int_0^{2\pi} z^{2-2n}\int_{-\pi/2}^{\pi/2}\cos^{2n-3}\zeta\,d\zeta d\theta$$

$$= \frac{\pi}{n-1}\int_0^{2\pi}(r\sin\theta\sin\phi+\rho)^{2-2n}\,d\theta.$$

By substituting $\theta' = \theta - \frac{\pi}{2}$ where $\theta' \in (0, 2\pi)$, we have

$$I_n = \frac{\pi}{n-1}\int_0^{2\pi}(r\cos\theta'\sin\phi+\rho)^{2-2n}\,d\theta'$$

$$= \frac{\pi}{n-1}\int_0^{2\pi}(r\sin\phi+\rho-2r\sin^2(\theta'/2)\sin\phi)^{2-2n}d\theta'.$$

Next, by introducing $t = \sin^2(\theta'/2)$ where $t \in (0,1)$, we get

$$I_n = \frac{2\pi}{n-1}\int_0^1(r\sin\phi+\rho-2rt\sin\phi)^{2-2n}\frac{1}{t^{1/2}(1-t)^{1/2}}\,dt$$

$$= \frac{2\pi}{n-1}(r\sin\phi+\rho)^{-2n+2}$$

$$\int_0^1 t^{-1/2}(1-t)^{-1/2}\left(1-\frac{2r\sin\phi}{r\sin\phi+\rho}t\right)^{-2n+2}dt. \quad (6)$$

Equation (6) can be written in the form

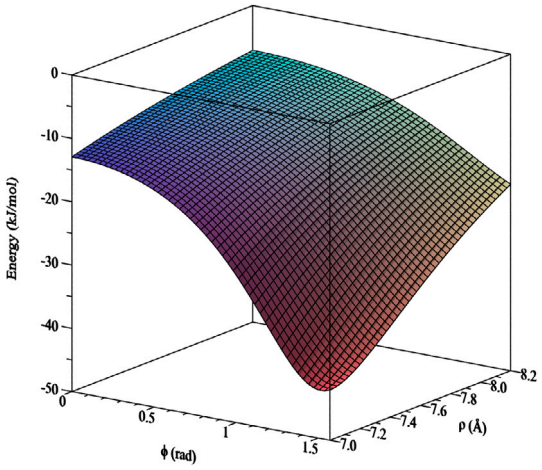

(a)

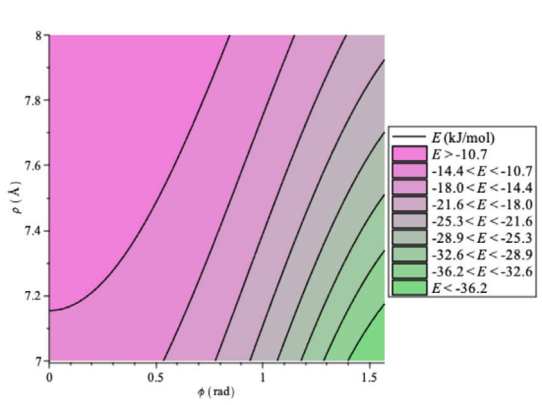

(b)

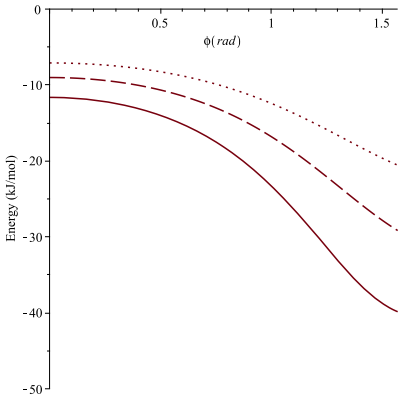

(c)

Fig. 11. The interaction energy between corannulene and graphene showing that for $\rho > 6.8$ Å, the energy is minimised when $\phi = \pi/2$ confirming that the standing bowl is the favourable configuration for this interval of ρ: (a) The total interaction energy as a function of ρ and ϕ, (b) Contour plot of the energy shown in (a) (the brightest green is the lowest energy region corresponding to ϕ close to $\pi/2$), and (c) The total energy as a function of ϕ for fixed values of $\rho = 7$ Å (solid line), $\rho = 7.5$ Å (dash line) and $\rho = 8$ Å (dotted line).

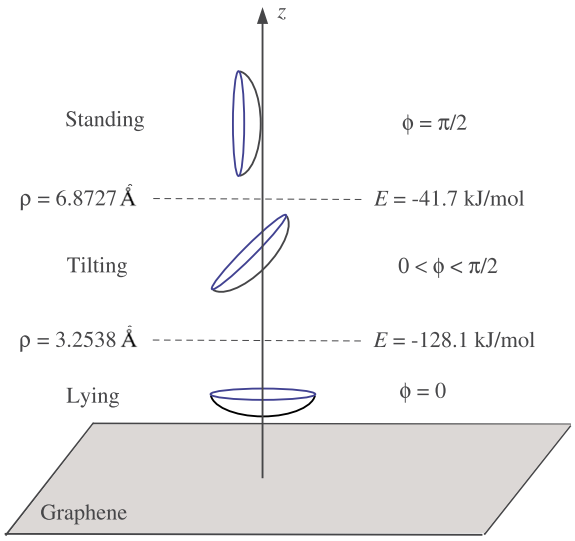

Fig. 12. Schematic diagram showing favourable orientations of corannulene concave-up bowl as the distance ρ from graphene sheet varies.

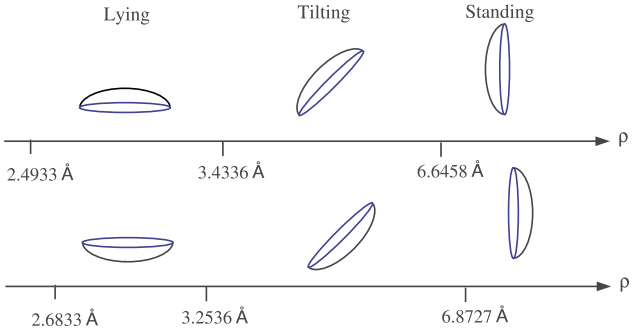

Fig. 13. The interval of the distance ρ corresponding to different orientations of corannulene.

$$I_n = \frac{2\pi^2}{n-1}(r\sin\phi + \rho)^{-2n+2} F\left(2n-2, \frac{1}{2}; 1; \frac{2r\sin\phi}{r\sin\phi + \rho}\right),$$

where $n = 3, 6$ and $F(a, b; c; z) = \sum_{k=0}^{\infty} \frac{(a)_k (b)_k}{k!(c)_k} z^k$ is the hypergeometric function where $(a)_k = a(a+1)(a+2)...(a+k-1)$ is the Pochhammer symbol.

References

[1] M. Jurícek, N.L. Strutt, J.C. Barnes, A.M. Butterfield, E.J. Dale, K.K. Baldridge, J.F. Stoddart, J.S. Siegel, Induced-fit catalysis of corannulene bowl-to-bowl inversion, Nat. Chem. 6 (2014) 222–228.

[2] A.A. Kroeger, A. Karton, Perylene bisimide cyclophanes as receptors for planar transition structures - catalysis of stereoinversions by shape-complementarity and noncovalent $\pi-\pi$ interactions, Org. Chem. Front. 8 (2021) 4408–4418.

[3] S. Ibáñez, E. Peris, Dimensional matching versus induced-fit distortions: binding affinities of planar and curved polyaromatic hydrocarbons with a tetragold metallorectangle, Angew. Chem. 59 (2020) 6860–6865.

[4] A. Karton, Inversion and rotation processes involving non-planar aromatic compounds catalyzed by extended polycyclic aromatic hydrocarbons, Chem. Phys. Lett. 614 (2014) 156–161.

[5] P.A. Denis, Pristine graphene-based catalysis: significant reduction of the inversion barriers of adsorbed and confined corannulene, sumanene, and dibenzo[a,g]corannulene, J. Phys. Chem. A 119 (2015) 5770–5777.

[6] A. Karton, Catalysis on pristine 2D materials via dispersion and electrostatic interactions, J. Phys. Chem. A 124 (2020) 6977.

[7] J. Wang, Z. Chen, B. Chen, Adsorption of polycyclic aromatic hydrocarbons by graphene and graphene oxide nanosheets, Environ. Sci. Technol. 48 (2014) 4817–4825.

[8] B. Collignon, P.N.M. Hoang, S. Picaud, D. Liotard, M.T. Rayez, J.C. Rayez, A semi-empirical potential model for calculating interactions between large aromatic molecules and graphite surfaces, J. Mol. Struct., Theochem 772 (2006) 1–12.

[9] F. Ortmann, W.G. Schmidt, F. Bechstedt, Attracted by long-range electron correlation: adenine on graphite, Phys. Rev. Lett. 95 (2005) 186101.

[10] D. Zhu, J. Pignatello, Characterization of aromatic compound sorptive interactions with black carbon (charcoal) assisted by graphite as a model, Environ. Sci. Technol. 39 (2005) 2033–2041.

[11] S.D. Chakarova-Käck, E. Schröder, B.I. Lundqvist, D.C. Langreth, Application of van der Waals density functional to an extended system: adsorption of benzene and naphthalene on graphite, Phys. Rev. Lett. 96 (2006) 146107.

[12] T. Tran-Duc, N. Thamwattana, B.J. Cox, J.M. Hill, Adsorption of polycyclic aromatic hydrocarbons on graphite surfaces, Comput. Mater. Sci. 49 (2010) S307–S312.

[13] V. Mehmeti, M. Sadiku, A comprehensive DFT investigation of the adsorption of polycyclic aromatic hydrocarbons onto graphene, Computation 10 (2022) 68.

[14] B. Li, P. Ou, Y. Wei, X. Zhang, J. Song, Polycyclic aromatic hydrocarbons adsorption onto graphene: a DFT and AIMD study, Materials 11 (2018) 726.

[15] O.V. Ershova, T.C. Lillestolen, E. Bichoutskaia, Study of polycyclic aromatic hydrocarbons adsorbed on graphene using density functional theory with empirical dispersion correction, Phys. Chem. Chem. Phys. 12 (2010) 6483–6491.

[16] P.A. Denis, Helicene adsorption on graphene, hexagonal boron nitride, graphane, and fluorographane, Chem. Phys. Lett. 806 (2022) 139998.

[17] M. Maruyama, S. Okada, All carbon p-n border in bilayer graphene by the molecular orientation of intercalated corannulene, J. Appl. Phys. 131 (2022) 134303.

[18] A.A. Kroeger, A. Karton, Catalysis by pure graphene—from supporting actor to protagonist through shape complementarity, J. Org. Chem. 84 (2019) 11343–11347.

[19] A.A. Kroeger, A. Karton, $\pi-\pi$ catalysis in carbon flatland—flipping [8]annulene on graphene, Chem. Eur. J. 27 (2021) 3420–3426.

[20] A.A. Kroeger, A. Karton, Graphene-induced planarization of cyclooctatetraene derivatives, J. Comput. Chem. 43 (2022) 96–105.

[21] P. Sripaturad, A. Karton, K. Stevens, N. Thamwattana, D. Baowan, B.J. Cox, Catalytic effect of graphene on the inversion of corannulene using a continuum approach with the Lennard-Jones potential, Nanoscale Adv. 5 (2023) 4571.

[22] D. Baowan, B.J. Cox, T.A. Hilder, J.M. Hill, N. Thamwattana, Modelling and Mechanics of Carbon-Based Nanostructured Materials, 1st edition, William Andrew, 2017.

[23] N. Thamwattana, A. Karton, P. Sripaturad, K. Stevens, D. Baowan, Orientation of corannulenes inside carbon nanotubes, Adv. Theory Simul. 2023 (2023) 2300554.

[24] T.S. Totton, A.J. Misquitta, M. Kraft, A first principles development of a general anisotropic potential for polycyclic aromatic hydrocarbons, J. Chem. Theory Comput. 6 (2010) 683–695.

[25] A.K. Rappe, C.J. Casewit, K.S. Colwell, W.A. Goddard III, W.M. Skiff, UFF, a full periodic table force field for molecular mechanics and molecular dynamics simulations, J. Am. Chem. Soc. 114 (1992) 10024–10035.

[26] Y. Zhao, D.G. Truhlar, Design of density functionals that are broadly accurate for thermochemistry, thermochemical kinetics, and nonbonded interactions, J. Phys. Chem. A 109 (2005) 5656.

[27] F. Weigend, R. Ahlrichs, Balanced basis sets of split valence, triple zeta valence and quadruple zeta valence quality for H to Rn: Design and assessment of accuracy, Phys. Chem. Chem. Phys. 7 (2005) 3297.

[28] L. Goerigk, S. Grimme, A thorough benchmark of density functional methods for general main group thermochemistry, kinetics, and noncovalent interactions, Phys. Chem. Chem. Phys. 13 (2011) 6670.

[29] L. Goerigk, A. Hansen, C. Bauer, S. Ehrlich, A. Najibi, S. Grimme, A look at the density functional theory zoo with the advanced GMTKN55 database for general main group thermochemistry, kinetics and noncovalent interactions, Phys. Chem. Chem. Phys. 19 (2017) 32184.

[30] A. Karton, How reliable is DFT in predicting relative energies of polycyclic aromatic hydrocarbon isomers? Comparison of functionals from different rungs of Jacob's ladder, J. Comput. Chem. 38 (2017) 370.

[31] L. Goerigk, R. Sharma, The INV24 test set: how well do quantum-chemical methods describe inversion and racemization barriers?, Can. J. Chem. 94 (2016) 1133.

[32] A. Karton, D. Gruzman, J.M.L. Martin, Benchmark thermochemistry of the C_nH_{2n+2} alkane isomers ($n = 2$–8) and performance of DFT and composite ab initio methods for dispersion-driven isomeric equilibria, J. Phys. Chem. A 113 (2009) 8434.

[33] A. Karton, A. Tarnopolsky, J.-F. Lamère, G.C. Schatz, J.M.L. Martin, Highly accurate first-principles benchmark datasets for the parametrization and validation of density functional and other approximate methods. Derivation of a robust, generally applicable, double-hybrid functional for thermochemistry and thermochemical kinetics, J. Phys. Chem. A 112 (2008) 12868.

[34] E. Caldeweyher, C. Bannwarth, S. Grimme, Extension of the D3 dispersion coefficient model, J. Chem. Phys. 147 (2017) 034112.

[35] E. Caldeweyher, S. Ehlert, A. Hansen, H. Neugebauer, S. Spicher, C. Bannwarth, S. Grimme, A generally applicable atomic-charge dependent London dispersion correction, J. Chem. Phys. 150 (2019) 154112.

[36] S.F. Boys, F. Bernardi, Calculation of small molecular interactions by differences of separate total energies – some procedures with reduced errors, Mol. Phys. 19 (1970) 553.

[37] H.B. Jansen, P. Ros, Non-empirical molecular orbital calculations on the protonation of carbon monoxide, Chem. Phys. Lett. 3 (1969) 140.

[38] B. Liu, A.D. Mclean, Accurate calculation of the attractive interaction of two ground state helium atoms, J. Chem. Phys. 59 (1973) 4557.

[39] M.J. Frisch, G.W. Trucks, H.B. Schlegel, G.E. Scuseria, M.A. Robb, J.R. Cheeseman, G. Scalmani, V. Barone, G.A. Petersson, H. Nakatsuji, X. Li, M. Caricato, A.V. Marenich, J. Bloino, B.G. Janesko, R. Gomperts, B. Mennucci, H.P. Hratchian, J.V. Ortiz, A.F. Izmaylov, J.L. Sonnenberg, D. Williams-Young, F. Ding, F. Lipparini, F. Egidi, J. Goings, B. Peng, A. Petrone, T. Henderson, D. Ranasinghe, V.G. Zakrzewski, J. Gao, N. Rega, G. Zheng, W. Liang, M. Hada, M. Ehara, K. Toyota, R. Fukuda, J. Hasegawa, M. Ishida, T. Nakajima, Y. Honda, O. Kitao, H. Nakai, T. Vreven, K. Throssell, J.A. Montgomery Jr, J.E. Peralta, F. Ogliaro, M.J. Bearpark, J.J. Heyd, E.N. Brothers, K.N. Kudin, V.N. Staroverov, T.A. Keith, R. Kobayashi, J. Normand, K. Raghavachari, A.P. Rendell, J.C. Burant, S.S. Iyengar, J. Tomasi, M. Cossi, J.M. Millam, M. Klene, C. Adamo, R. Cammi, J.W. Ochterski, R.L. Martin, K. Morokuma, O. Farkas, J.B. Foresman, D.J. Fox, Gaussian 16 Revision C.01, Gaussian Inc., Wallingford CT, 2016.

[40] A. Karton, $\pi-\pi$ interactions between benzene and graphene by means of large-scale DFT-D4 calculations, Chem. Phys. 561 (2022) 111606.

[41] J.A. Rackers, J.W. Ponder, Classical Pauli repulsion: an anisotropic, atomic multipole model, J. Chem. Phys. 150 (2019) 084104.

[42] Y. Jin, E.R. Johnson, X. Hu, W. Yang, H. Hu, Contributions of Pauli repulsions to the energetics and physical properties computed in QM/MM methods, J. Comput. Chem. 34 (2013) 2380–2388.